Identification of plastic deformations and parameters of nonlinear single-bay frames

Francis T.K. Au[*] and Z.H. Yan[a]

Department of Civil Engineering, The University of Hong Kong, Pokfulam Road, Hong Kong, P.R. China

Abstract. This paper presents a novel time-domain method for the identification of plastic rotations and stiffness parameters of single-bay frames with nonlinear plastic hinges. Each plastic hinge is modelled as a pseudo-semi-rigid connection with nonlinear hysteretic moment-curvature characteristics at an element end. Through the comparison of the identified end rotations of members that are connected together, the plastic rotation that furnishes information of the locations and plasticity degrees of plastic hinges can be identified. The force consideration of the frame members may be used to relate the stiffness parameters to the elastic rotations and the excitation. The damped-least-squares method and damped-and-weighted-least-squares method are adopted to estimate the stiffness parameters of frames. A noise-removal strategy employing a de-noising technique based on wavelet packets with a smoothing process is used to filter out the noise for the parameter estimation. The numerical examples show that the proposed method can identify the plastic rotations and the stiffness parameters using measurements with reasonable level of noise. The unknown excitation can also be estimated with acceptable accuracy. The advantages and disadvantages of both parameter estimation methods are discussed.

Keywords: nonlinear single-bay frames; parameters estimation; plastic rotation; stiffness parameter; unknown excitation

1. Introduction

Under extreme events such as earthquakes and typhoons, plastic hinges may form in a steel structure. After these extreme events, it is not easy to assess the structural damage due to the formation of plastic hinges. Normally the assessment of structural conditions relies upon the structural responses as an important source of information. However, the responses and the state of the structure during these extreme events are complicated because of the occurrence of yielding, unloading, reloading, etc. especially around the plastic hinges. Therefore better understanding of such complicated structural behaviour during extreme events is valuable for engineers to assess the structural conditions and to make the necessary decisions for retrofitting.

The parameters to describe structural behaviour can be physical parameters such as stiffness, damping, etc. or modal parameters like frequency, mode shape, etc. Many techniques have been developed recently for modal parameter estimation (Park *et al.* 2011, Ye *et al.* 2012, Zhang *et al.* 2013, Yang *et al.* 2014, Nagarajaiah and Yang 2015). Compared with the modal parameters, the physical parameters can reflect the integrity of structures more directly. Physical parameters can also reflect better the complicated nonlinear behaviour of structures during extreme events including various nonlinear characteristics and damage representing the degraded state. Some researchers have identified physical parameters from modal

information (Burak and Ram 2001, Chakraverty 2005), but unfortunately certain information may be lost during the solution for the modal information and the physical parameters identified from modal information cannot reflect the structural degradation. As a result, direct estimation of physical parameters from the time domain has become popular. Shi *et al.* (2007) presented a physical parameter identification method for linear time-varying systems based on the subspace technique. Lu and Law (2007) presented a method based on the sensitivity of structural responses to identify both the system parameters and the input excitation force of a structure. Kang *et al.* (2005) presented a system identification scheme in time domain to estimate the stiffness and damping parameters of a structures using measured acceleration. Later the method was extended to the detection of sudden structural damage that occurs during an earthquake based on the moving time window technique (Park *et al.* 2008). Wang *et al.* (2014) presented a method based on discrete wavelet transform for time-varying physical parameter identification of shear type structures. Huang *et al.* (2015) presented techniques based on the least square estimation combined with the substructure approach to identify the parameters of a cable-stayed bridge with a large number of degrees of freedom.

As normally the external excitations have not been measured or are not available, Yang *et al.* (2009) presented a method with adaptive quadratic sum-square error and unknown inputs for identification of time-varying and hysteretic structures. The method was applied to identify the time-varying structural parameters of reinforced concrete frame (Yang *et al.* 2014a) and damage to bolted connection of a steel frame (Yang *et al.* 2014b). Al-Hussein and Haldar (2015a) presented a method of unscented Kalman filter with unknown input to identify defects at the

---

*Corresponding author, Ph.D., Professor
  E-mail: francis.au@hku.hk
[a] Ph.D.

local element level using only a limited amount of noise-contaminated nonlinear response information and without excitations. The accuracy of method was further improved using unscented Kalman filter with unknown input and weighted global iteration for defect identification within a defective element (Al-Hussein and Haldar 2015b).

In the above studies, the hysteretic models to describe damage have been mostly based on linear or linear time-varying parameters, and there has been relatively little work focusing on the identification of nonlinear structural behaviour. Normally during extreme events, the plastic hinges with hysteretic properties govern the behaviour of frames. The plastic deformations at plastic hinges are key indicators to assess the structural conditions. In order to study such complicated behaviour and to provide a direction for engineers to assess the structural conditions for necessary retrofitting, a novel method is proposed for identification and parameter estimation of frames with hysteretic plastic hinges. Only single-bay frames with relatively few degrees of static indeterminacy are initially chosen for investigation of the proposed method. The basic idea in this paper is to treat nonlinear frames as a combination of linear members and hysteretic plastic hinges. Through comparison of the identified end rotations of members connected together, the plastic rotation which furnishes information of the location and plasticity degree of plastic hinges can be calculated. The force consideration of the frame members may be used to relate the stiffness parameters to the elastic rotations and the excitation. The stiffness parameters can be estimated based on the equation constructed through the damped-least-squares (DLS) method and the damped-and-weighted-least-squares (DWLS) method (Tikhonov 1963). The scenarios with unknown input are also investigated. Numerical examples including a portal frame and a two-storey frame show that the proposed method can identify the plastic rotations and estimate the stiffness parameters with satisfactory accuracy. The horizontal excitation can be estimated with certain accuracy when it is not available.

2. Modelling of members

In order to simulate the members with hysteretic plastic hinges, the semi-rigid technique for modelling of plastic hinges in members (Au and Yan 2008) is adopted. In this study, only material nonlinearity is considered. A brief summary of the essential points in the method adopted by Au and Yan (2008) is presented here.
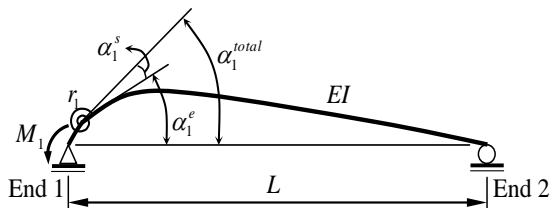

Fig. 1 Concept of fixity factor

Monforton and Wu (1963) modelled the semi-rigid connection as a zero-length linear spring at each end of a member as shown in Fig. 1 and presented the fixity factor λ_i at end i of the member as

$$\lambda_i = \frac{\alpha_i^e}{\alpha_i^e + \alpha_i^s} = \frac{\alpha_i^e}{\alpha_i^{total}} = \frac{1}{1 + 3EI/r_i L} \qquad (i = 1, 2) \qquad (1)$$

where α_i^e is the elastic end-rotation at end i, α_i^s is the spring rotation at end i, α_i^{total} is the total end-rotation at end i, r_i is the rotational stiffness of the semi-rigid connection at end i, E is elastic modulus of the member, I is moment of inertia of the member, and L is the length of the member. A plasticity factor can be introduced based on the fixity factor to describe the behaviour of a plastic hinge from the initial elastic state to the plastic state under monotonic loading. The plasticity factor (Hasan *et al.* 2002) can be defined as

$$p_i = \frac{1}{1 + 3EI / (L \, dM_i / d\alpha_i^p)} \qquad (2)$$

The stiffness matrix $\mathbf{K}$ of a member with hysteretic plastic hinges can be expressed in the form of plasticity factors by replacing the fixity factors λ_i $(i = 1,2)$ with the plasticity factors p_i $(i = 1,2)$ as

$$\mathbf{K} = \mathbf{K}_e \mathbf{S}_e^p \qquad (3)$$

where $\mathbf{S}_e^p$ is the corresponding correction matrix, and $\mathbf{K}_e$ is the standard elastic stiffness matrix (Au and Yan 2008).

3. Identification of nonlinear single-bar frames

3.1 Identification of plastic rotations

Each frame is considered as a combination of linear members and hysteretic plastic hinges. It is reasonable to assume that, for this kind of frames, not all members connected together will yield simultaneously during the whole dynamic process. Usually the beams and columns connected together are of different sizes and so are their yielding moments. The displacements of structural members are used in the formulation of problem. While it is more convenient in actual applications to measure vibrations by accelerometers, reasonably accurate estimates of the displacement time histories can be obtained by successive integration of the acceleration time histories with proper correction (Gindy *et al.* 2016) by velocity estimation method, linear baseline correction method, or the use of a suitable high pass filter or "omega arithmetic".

The displacement $u(z,t)$ of a beam can be described by a linear combination of interpolation functions as

$$u(z,t) = v_1(t)H_1(z) + \alpha_1(t)H_2(z) + v_2(t)H_3(z) + \alpha_2(t)H_4(z) \quad (4)$$

where z is the distance from end 1, $v_i(t)$ and $\alpha_i(t)$ $(i=1,2)$ are the end displacements and rotations respectively,

and $H_i(z)$ $(i=1,2,3,4)$ are the interpolation functions for a uniform beam of length L as follow

$$\begin{cases} H_1(z) = 1 - 3\left(\dfrac{z}{L}\right)^2 + 2\left(\dfrac{z}{L}\right)^3 \\ H_2(z) = L\left(\dfrac{z}{L}\right) - 2L\left(\dfrac{z}{L}\right)^2 + L\left(\dfrac{z}{L}\right)^3 \\ H_3(z) = 3\left(\dfrac{z}{L}\right)^2 - 2\left(\dfrac{z}{L}\right)^3 \\ H_4(z) = -L\left(\dfrac{z}{L}\right)^2 + L\left(\dfrac{z}{L}\right)^3 \end{cases} \tag{5}$$

If there are four displacement measurements, namely $u(z_1,t)$, $u(z_2,t)$, $u(z_3,t)$ and $u(z_4,t)$, perpendicular to the member at different locations z_1, z_2, z_3 and z_4, these displacements can be expressed as

$$\begin{bmatrix} u(z_1,t) \\ u(z_2,t) \\ u(z_3,t) \\ u(z_4,t) \end{bmatrix} = \begin{bmatrix} H_1(z_1) & H_2(z_1) & H_3(z_1) & H_4(z_1) \\ H_1(z_2) & H_2(z_2) & H_3(z_2) & H_4(z_2) \\ H_1(z_3) & H_2(z_3) & H_3(z_3) & H_4(z_3) \\ H_1(z_4) & H_2(z_4) & H_3(z_4) & H_4(z_4) \end{bmatrix} \begin{bmatrix} v_1(t) \\ \alpha_1(t) \\ v_2(t) \\ \alpha_2(t) \end{bmatrix} \tag{6}$$

or in matrix form as

$$\mathbf{u} = \mathbf{H}\boldsymbol{\varphi} \tag{7}$$

Then the displacements at the member ends can be solved as

$$\boldsymbol{\varphi} = \mathbf{H}^{-1}\mathbf{u} \tag{8}$$

The deformation of a member under external bending moments is shown in Fig. 2. It is assumed that no loading is applied on the member except for the ends. The variable α_i^{total} denotes the total rotation at end i of the member under external loading, α_i^e is the elastic rotation at the end, and α_i^p is the plastic rotation there. Before the application of loading (i.e., the initial configuration of member at time $t = 0$), the orientation of the member is denoted by θ_0 that is the counter-clockwise angle of rotation so that the global *X*-axis becomes parallel to the initial element *x*-axis. At the time considered (i.e., the deformed configuration of member at time $t + \Delta t$), due to the effect of loading, the member adopts a deformed configuration with an updated member *x'*-axis pointing from end 1 to end 2. The orientation of the updated member *x'*-axis is defined by θ_t that is the counter-clockwise angle of rotation so that the global *X*-axis becomes parallel to the updated element *x'*-axis. The incremental rotation from θ_0 to θ_t is then denoted by $\Delta\theta$. By reference to Fig. 2 (Au and Yan 2008), the elastic rotation α_i^e at end i of the member is given by

$$\alpha_i^e = \alpha_i^{total} - \alpha_i^p - \Delta\theta \tag{9}$$
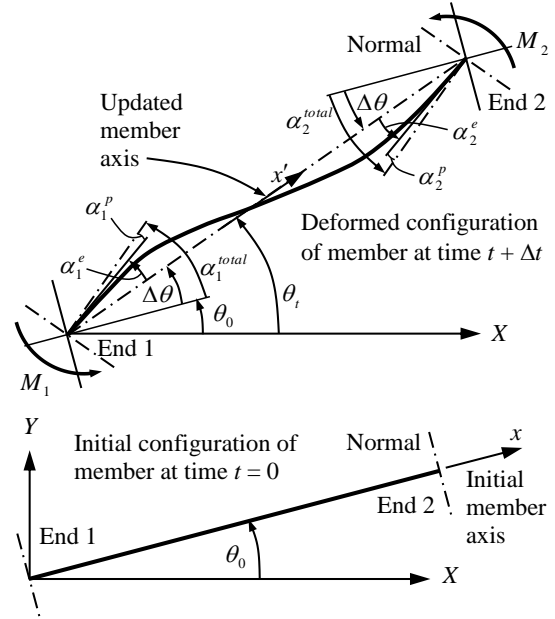

Fig. 2 Deformation of member with plastic hinge

The identified end rotation $\alpha_i^{identified}$ from Eq. (8) should be the sum of elastic rotation α_i^e and incremental rotation $\Delta\theta$ at the end, which is also equal to the total rotation α_i^{total} minus the plastic rotation α_i^p, namely

$$\alpha_i^{identified} = \alpha_i^e + \Delta\theta = \alpha_i^{total} - \alpha_i^p \tag{10}$$

The total rotation α_i^{total} should be the same for all the members connected at end i. Therefore, the plastic rotation can be calculated by comparing the identified end rotations of two members in which only one yields during the dynamic process. So far, the procedure has not made use of any excitation information or structural model of the frames.

3.2 Estimation of stiffness parameters

Besides plastic rotations, the member stiffness is also required for further investigation of structural safety. According to Eq. (10), the elastic rotation can be calculated as

$$\alpha_i^e = \alpha_i^{identified} - \Delta\theta \tag{11}$$

while the elastic rotation α_i^e can be evaluated from the end moments M_i and M_j as

$$\alpha_i^e = \frac{M_i L}{3EI} - \frac{M_j L}{6EI} \quad \text{for } i = 1, j = 2 \text{ or } i = 2, j = 1 \tag{12}$$

For convenience, the stiffness parameter k of member is defined in terms of the flexural rigidity EI and length L as

$$k = \frac{EI}{L} \tag{13}$$

For both member ends, the end moments M_i can be calculated as

$$M_i = 4k\alpha_i^e + 2k\alpha_j^e \quad \text{for } i=1, j=2 \text{ or } i=2, j=1 \quad (14)$$

Suppose that the single-bay frame in Fig. 3 is subject to a horizontal earthquake excitation. For convenience, the columns supporting floor q together with the beam itself are collectively called storey q. If the rotational inertial effect of the beam and slab is ignored, the bending moments alone should satisfy the following rotational equation of motion at each beam-column joint

$$\sum_{d=1}^{N^J} M_d^J = 0 \quad (15)$$

where M_d^J is the bending moment of member d at joint J of the frame, and N^J is the total number of the members connected together at joint J. Besides, the inertial force, damping force, shear force and the excitation force at each storey should also satisfy the following equation of horizontal motion

$$\sum_{d=1}^{N^q} F_d^q + \sum_{\tau=q}^{n_s} \left(m_\tau \ddot{x}_\tau^h + c_\tau \dot{x}_\tau^h + m_\tau \ddot{x}_g \right) = 0 \quad (16)$$

where F_d^q is the shear force of member d at floor q of the frame, N^q is the total number of columns supporting floor q, m_τ and c_τ are the lumped mass and damping of floor τ $(\tau = q, q+1, \cdots, n_s)$, n_s is the total number of floors, $\ddot{x}_\tau^h$ and $\dot{x}_\tau^h$ are the horizontal acceleration and velocity of the beam at floor τ $(\tau = q, q+1, \cdots, n_s)$, and $\ddot{x}_g$ is the measured external earthquake excitation. Therefore to estimate the stiffness parameters of the $3n_s$ members, $3n_s$ equations of motion are necessary. For each floor, they include two for the rotational motion of the beam-column joints and one for the horizontal motion. The system of equations of motion can be established as follows

Fig. 3 A general single-bay frame

$$\text{where} \begin{cases} D_{cLiq}^M = 4\alpha_{cLiq}^e + 2\alpha_{cLjq}^e \\ D_{cRiq}^M = 4\alpha_{cRiq}^e + 2\alpha_{cRjq}^e \\ D_{biq}^M = 4\alpha_{biq}^e + 2\alpha_{bjq}^e \\ D_{cLq}^S = -\dfrac{6\left(\alpha_{cLiq}^e + \alpha_{cLjq}^e\right)}{h_q} \\ D_{cRq}^S = -\dfrac{6\left(\alpha_{cRiq}^e + \alpha_{cRjq}^e\right)}{h_q} \\ D_q^d = \displaystyle\sum_{\tau=q}^{n_s}\left(m_\tau \ddot{x}_\tau^h + c_\tau \dot{x}_\tau^h + m_\tau \ddot{x}_g\right) \end{cases}$$

for $i=1, j=2$ or $i=2, j=1$, and $q=1, 2, \cdots, n_s$

or in matrix form as

$$\bar{\mathbf{A}}_{3n_s \times 3n_s} \mathbf{\gamma}_{3n_s \times 1} = \bar{\mathbf{b}}_{3n_s \times 1} \quad (18)$$

$$\begin{bmatrix} D_{cL2n_s}^M & 0 & D_{b1n_s}^M & 0 & 0 & 0 & \cdots & 0 & 0 & 0 & 0 & 0 & 0 \\ 0 & D_{cR2n_s}^M & D_{b2n_s}^M & 0 & 0 & 0 & \cdots & 0 & 0 & 0 & 0 & 0 & 0 \\ D_{cLn_s}^S & D_{cRn_s}^S & 0 & 0 & 0 & 0 & \cdots & 0 & 0 & 0 & 0 & 0 & 0 \\ D_{cL1n_s}^M & 0 & 0 & D_{cL2(n_s-1)}^M & 0 & D_{b1(n_s-1)}^M & \cdots & 0 & 0 & 0 & 0 & 0 & 0 \\ 0 & D_{cR1n_s}^M & 0 & 0 & D_{cR2(n_s-1)}^M & D_{b2(n_s-1)}^M & \cdots & 0 & 0 & 0 & 0 & 0 & 0 \\ 0 & 0 & 0 & D_{cL(n_s-1)}^S & D_{cR(n_s-1)}^S & 0 & \cdots & 0 & 0 & 0 & 0 & 0 & 0 \\ \vdots & \vdots & \vdots & \vdots & \vdots & \vdots & \cdots & \vdots & \vdots & \vdots & \vdots & \vdots & \vdots \\ 0 & 0 & 0 & 0 & 0 & 0 & \cdots & D_{cL22}^M & 0 & D_{b12}^M & 0 & 0 & 0 \\ 0 & 0 & 0 & 0 & 0 & 0 & \cdots & 0 & D_{cR22}^M & D_{b22}^M & 0 & 0 & 0 \\ 0 & 0 & 0 & 0 & 0 & 0 & \cdots & D_{cL2}^S & D_{cR2}^S & 0 & 0 & 0 & 0 \\ 0 & 0 & 0 & 0 & 0 & 0 & \cdots & D_{cL12}^M & 0 & 0 & D_{cL21}^M & 0 & D_{b11}^M \\ 0 & 0 & 0 & 0 & 0 & 0 & \cdots & 0 & D_{cR12}^M & 0 & 0 & D_{cR21}^M & D_{b21}^M \\ 0 & 0 & 0 & 0 & 0 & 0 & \cdots & 0 & 0 & 0 & D_{cL1}^S & D_{cR1}^S & 0 \end{bmatrix} \begin{Bmatrix} k_{cLn_s} \\ k_{cRn_s} \\ k_{bn_s} \\ k_{cL(n_s-1)} \\ k_{cR(n_s-1)} \\ k_{b(n_s-1)} \\ \vdots \\ k_{cL2} \\ k_{cR2} \\ k_{b2} \\ k_{cL1} \\ k_{cR1} \\ k_{b1} \end{Bmatrix} = \begin{Bmatrix} 0 \\ 0 \\ D_{n_s}^d \\ 0 \\ 0 \\ D_{(n_s-1)}^d \\ \vdots \\ 0 \\ 0 \\ D_2^d \\ 0 \\ 0 \\ D_1^d \end{Bmatrix} \quad (17)$$
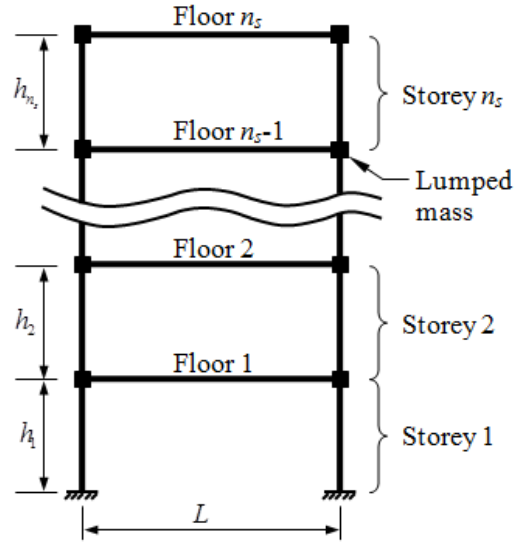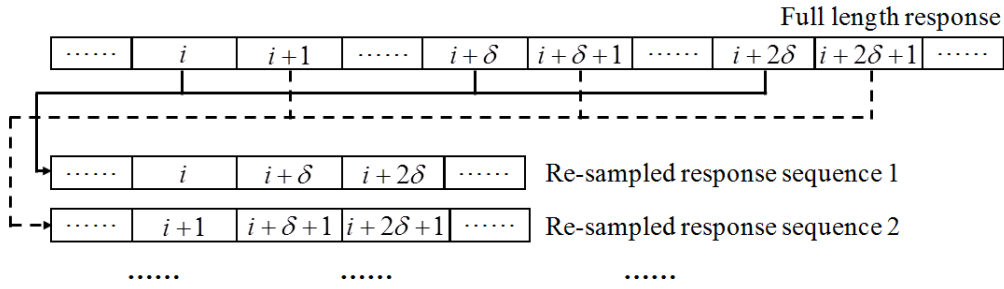
Full length response

Fig. 4 Illustration of the response selection scheme

where k_{cLq}, k_{cRq} and k_{bq} $(q = 1, 2, \cdots, n_s)$ are stiffness parameters of the left column (*cL*) and right column (*cR*) below floor q and the beam (*b*) at floor q respectively, α^e_{cLiq}, α^e_{cRiq} and α^e_{biq} $(q = 1, 2, \cdots, n_s)$ are elastic rotations at end i of the left and right columns below floor q and the beam at floor q respectively, and h_q $(q = 1, 2, \cdots, n_s)$ is the storey height below floor q.

3.3 Damped-least-squares method and damped-and-weighted-least-squares method

If the whole dynamic process is divided into n_t equal time steps of duration Δt, Eq. (18) can be established for all the time steps as

$$\mathbf{A}_{(n_t \times 3n_s) \times 3n_s} \boldsymbol{\gamma}_{3n_s \times 1} = \mathbf{b}_{(n_t \times 3n_s) \times 1} \tag{19}$$

To solve Eq. (19), usually the least-squares-method is adopted. Like common inverse problems, the results from the straightforward least squares method will be ill-conditioned. In order to provide bounds to the solution, the DLS method (Tikhonov 1963) is adopted, namely

$$\boldsymbol{\gamma} = \left(\mathbf{A}^T \mathbf{A} + \rho \mathbf{I} \right)^{-1} \mathbf{A}^T \mathbf{b} \tag{20}$$

where ρ is a non-negative damping coefficient governing the participation of least-squares error in the solution, $\mathbf{I}$ is the identity matrix and the dimensions have been dropped for brevity. In Eq. (17), the horizontal equations of motion resulting from Eq. (16) contain more measurement information than that of the moment equations resulting from Eq. (15). Therefore during the solution of Eq. (17) for the stiffness parameters, the horizontal equations of motion can be given more weight than the moment equations. The weighted-least-squares method is adopted in conjunction with the DLS method, thereby resulting in the DWLS method as

$$\boldsymbol{\gamma} = \left(\mathbf{A}^T \mathbf{W} \mathbf{A} + \rho \mathbf{I} \right)^{-1} \mathbf{A}^T \mathbf{W} \mathbf{b} \tag{21}$$

where $\mathbf{W}$ is the weight matrix giving the corresponding importance to the related equations. The size of weight matrix $\mathbf{W}$ is quite large because of the large row size of matrix $\mathbf{A}$. In the implementation of the DWLS method, a response selection scheme is adopted to choose the response at certain intervals characterised by the integer δ. As shown in Fig. 4, the full length response can be re-sampled as several shorter response sequences. Each re-sampled response sequence can be used for the estimation of stiffness parameters. The average value of the results from various re-sampled response sequences can be taken as the final result.

In practice, the excitation may not be available, but the proposed method can still be applied to reconstruct the excitation approximately. The excitation time history is initially taken to be identically zero. The stiffness parameters can be approximately estimated using Eq. (20) as

$$\hat{\boldsymbol{\gamma}} = \left(\mathbf{A}^T \mathbf{A} + \rho \mathbf{I} \right)^{-1} \mathbf{A}^T \hat{\mathbf{b}} \tag{22}$$

or using Eq. (21) as

$$\hat{\boldsymbol{\gamma}} = \left(\mathbf{A}^T \mathbf{W} \mathbf{A} + \rho \mathbf{I} \right)^{-1} \mathbf{A}^T \mathbf{W} \hat{\mathbf{b}} \tag{23}$$

where $\hat{\mathbf{b}}$ is the same as $\mathbf{b}$ except that the ground acceleration $\ddot{x}_g$ in Eq. (17) is taken to be identically zero. Then incorporating the identified initial stiffness parameters $\hat{\boldsymbol{\gamma}}$ into Eq. (19), the external excitation can be estimated. In Eq. (21) or (23), the weight matrix $\mathbf{W}$ can be determined to suit various scenarios as elaborated later.

3.4 Noise-removal technique

In Eq. (19), the information in matrix $\mathbf{A}$ used in the stiffness parameter estimation is mostly composed of elastic rotations extracted from the measured responses. From the measurements to the elastic rotations used in parameter estimation, the measurement noise tends to propagate and adversely affect the estimation of elastic rotations. Noise is first removed from the noise-contaminated response using the de-noising technique based on wavelet packets provided by MATLAB. Then a smoothing process based on the moving time window technique (Park *et al.* 2008) is carried out as shown in Fig. 5. A moving time window is gradually shifted from the beginning of response. The average value of response in the moving time window is calculated and then taken as the smoothed response at the middle of window. After the moving time window has swept through
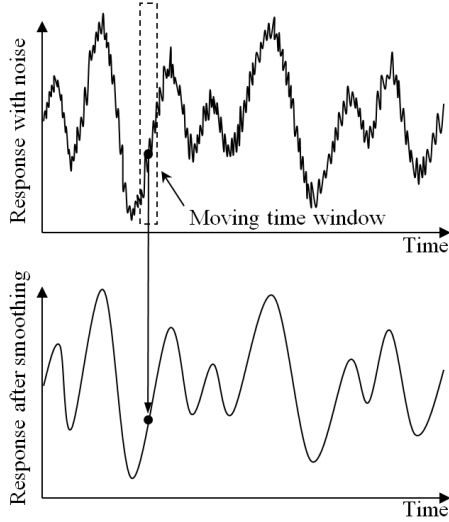
Fig. 5 Smoothing by moving time window

Fig. 6 Example 1: A portal frame for verification and illustration (↔ : sensor with measurement direction indicated)

Table 1 Example 1: Properties of steel W-type I-beams used

Member	Area (m^2)	Moment of Inertia (m^4)	Yield Moment (Nm)
Column (W21×93)	1.7613×10^{-2}	8.6160×10^{-4}	8.9814×10^{5}
Beam (W12×87)	1.6516×10^{-2}	3.0801×10^{-4}	5.3645×10^{5}

the whole response, the small spikes caused by the noise can be smoothed as shown in Fig. 5.

4. Numerical examples

Examples including a portal frame and a single-bay two-storey frame under horizontal excitations are described here. Unless otherwise stated, the Young's modulus is 2×10^{11} N/m^2 while the yield stress is 2.48×10^{8} N/m^2. Mass-proportional damping is assumed, and the critical damping ratio is taken to be 5%. For simplicity, the rotational inertial effect of the beam and slab is ignored and the lumped mass matrix is adopted. For convenience, PPHL denotes "potential plastic hinge location". At the beam-column joint, the column with higher bending capacity than the beam is less likely to yield.

4.1 Example 1: A portal frame

A portal frame made up of steel W-type I-beam, as shown in Fig. 6, is used for verification and illustration of the proposed method. The properties of the steel W-type I-beams are given in Table 1. At each of the beam-column joints, a 70,000 kg mass point is provided to simulate the floor mass together with a vertically downward load of 700 kN to account for gravity. The beam and columns are discretized into elements 0.5m in length. The assumed excitation is that of the El Centro earthquake with magnified peak ground acceleration of 0.5 *g*, where *g* is the acceleration due to gravity. The sampling frequency is 1000 Hz for all measurements. Fig. 6 shows an arbitrary arrangement of sensors for measurement. All measurements are supposed to be taken relative to the ground. Therefore the relative displacement at the column base can be taken as zero. As only horizontal excitation is considered and the axial deformations are much less significant than bending deformations, the vertical displacement at each beam-column joint can be taken as zero, which is a reasonable
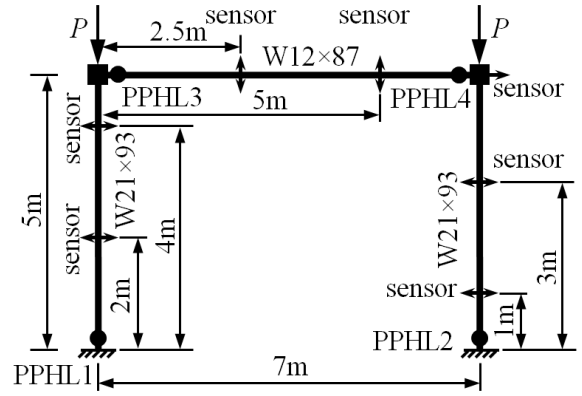
approximation to enable reduction of sensors. Similarly the horizontal displacements at beam-column joints of the same floor are also regarded as the same, which requires measurement at one location only. Therefore only two sensors are required in each member for measurement of displacements perpendicular to member axis. In particular, the horizontal acceleration and velocity of the beam are also needed for the estimation of stiffness parameters.

The proposed method is first examined based on simulated measurements without noise. The noise-removal technique is not applied. By comparing the identified end rotation from Eq. (8), the plastic rotations at selected plastic hinges can be identified as shown in Fig. 7. The fluctuations of result at PPHL3 are primarily due to the assumption of zero vertical displacement at beam-column joints. It shows that the plastic rotation can be identified by the proposed method using simulated measurements without noise.

In the parameter estimation, both the DLS and DWLS methods are adopted, and the results are compared. The damping coefficient in Eqs. (20)-(23) is chosen as $\rho = 1 \times 10^{-7}$. For the portal frame, the weight matrix **W** is defined as

$$\mathbf{W} = \begin{bmatrix} \bar{\mathbf{W}}_1 & \cdots & 0 & 0 & 0 \\ \vdots & \ddots & 0 & 0 & 0 \\ 0 & 0 & \bar{\mathbf{W}}_t & 0 & 0 \\ 0 & 0 & 0 & \ddots & \vdots \\ 0 & 0 & 0 & \cdots & \bar{\mathbf{W}}_{n_t} \end{bmatrix} \quad (24)$$

where the sub-matrix $\bar{\mathbf{W}}_t$ to apply weights on the two moment equations and the horizontal equation of motion of each floor is given by

Table 2 Example 1: Identified stiffness parameters (Unit: Nm; zero noise)

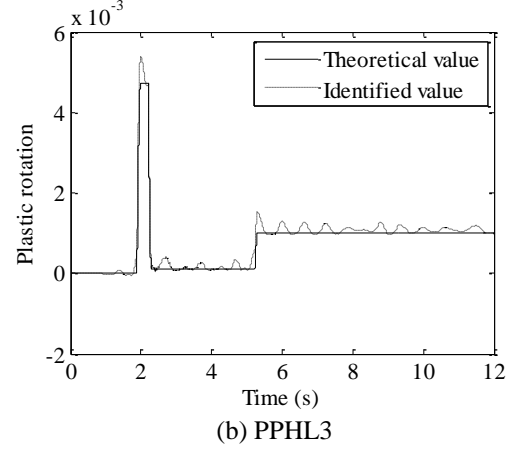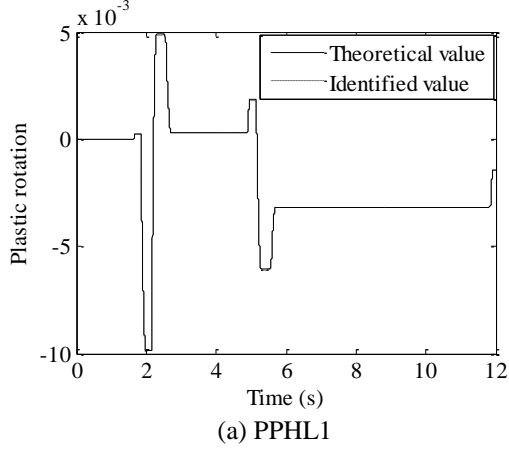|	Theoretical value	DLS with known excitation	DWLS with known excitation	DLS with unknown excitation	DWLS with unknown excitation
k_{c1}	3.4464×10^7	3.4435×10^7 (0.08%)	3.4431×10^7 (0.10%)	3.2455×10^7 (5.83%)	3.2525×10^7 (5.63%)
k_{c2}	3.4464×10^7	3.4494×10^7 (0.09%)	3.4518×10^7 (0.16%)	3.2487×10^7 (5.74%)	3.2374×10^7 (6.06%)
k_b	0.8800×10^7	0.8904×10^7 (1.18%)	0.8906×10^7 (1.20%)	0.8388×10^7 (4.68%)	0.8383×10^7 (4.74%)

(a) PPHL1

(b) PPHL3

Fig. 7 Example 1: Plastic rotations at selected plastic hinges (zero-noise scenario)

$$\overline{\mathbf{W}}_t = \begin{bmatrix} 0.1 & 0 & 0 \\ 0 & 0.1 & 0 \\ 0 & 0 & 1 \end{bmatrix} \text{ for } t = 1, 2, \cdots n_t \qquad (25)$$

In other words, more weight is placed on the horizontal equations of motion as they involve more measurements. The response selection scheme adopted for the DWLS method is characterised by a value of δ that is equivalent to a time interval of 0.012s. There are 12 re-sampled response sequences each with 1000 time points. The DWLS method is then applied to each of them. The estimated stiffness parameters by averaging the individual results are shown in Table 2, together with the percentage errors calculated based on the absolute value of deviation from the theoretical value. Table 2 shows that for the zero-noise scenario, results from both the DWLS and DLS methods are nearly the same. In this case, the results from the DLS method are slightly better for most stiffness parameters as it uses all data together for estimation, while the DWLS method adopts smaller sets of re-sampled data for estimation before averaging them. Table 2 also shows that even though the excitation is unknown, the stiffness parameters can still be estimated with acceptable accuracy under zero-noise condition. The estimated earthquake excitations from both the DLS and DWLS methods are presented in Fig. 8, which shows that both work satisfactorily under zero-noise condition.

In order to evaluate the sensitivity of the proposed method to noise, random noise is added to the simulated noise-free measurement vector $\mathbf{y}_{nf}$ to form the simulated noise-polluted measurement vector $\mathbf{y}_{np}$ as (Au *et al.* 2004)
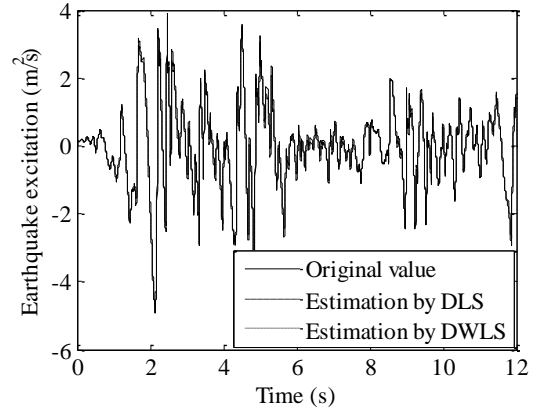

Fig. 8 Example 1: Estimated earthquake excitations (zero-noise scenario)

$$\mathbf{y}_{np} = \mathbf{y}_{nf} + \text{RMS}(\mathbf{y}_{nf}) \cdot N_{level} \cdot \mathbf{R} \qquad (26)$$

where $\text{RMS}(\mathbf{y}_{nf})$ is the root-mean-square value of the noise-free measurement vector $\mathbf{y}_{nf}$, N_{level} is the noise level, and $\mathbf{R}$ is the random noise vector with zero mean and unit standard deviation. In the present study, 2.5% noise level is adopted. The noise-removal technique mentioned above is applied before the measurements go into the identification process. The width of the moving time window is 0.15s.

Table 3 Example 1: Identified stiffness parameters (Unit: Nm; 2.5% noise)

	Theoretical value	DLS with known excitation	DWLS with known excitation	DLS with unknown excitation	DWLS with unknown excitation
k_{c1}	3.4464×10^7	3.3870×10^7 (1.72%)	3.3945×10^7 (1.51%)	3.0312×10^7 (12.05%)	2.9925×10^7 (13.17%)
k_{c2}	3.4464×10^7	3.4523×10^7 (0.17%)	3.4850×10^7 (1.12%)	3.0999×10^7 (10.05%)	3.1749×10^7 (7.88%)
k_b	0.8800×10^7	0.8846×10^7 (0.52%)	0.8898×10^7 (1.11%)	0.7930×10^7 (9.89%)	0.7977×10^7 (9.35%)
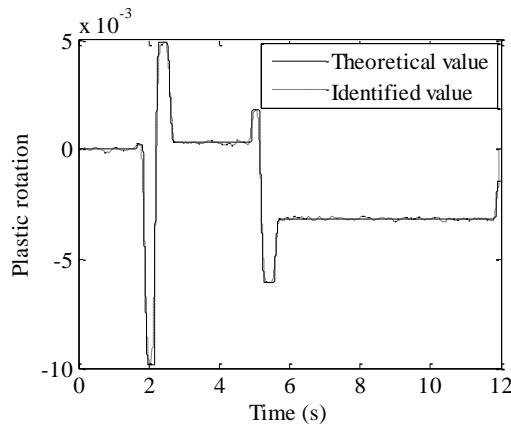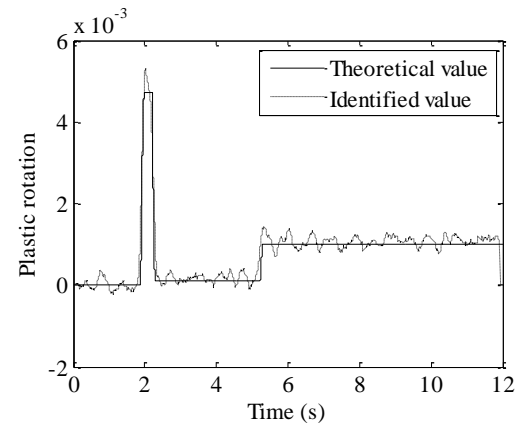
(a) PPHL1   (b) PPHL3

Fig. 9 Example 1: Plastic rotations at selected plastic hinges (2.5% noise)

The other conditions are the same as before. The identified plastic rotations at selected plastic hinges are shown in Fig. 9, which shows that the method works with measurements contaminated with noise. The estimated stiffness parameters from different methods are shown in Table 3 while, for the case of unknown excitation, the estimated earthquake excitations are shown in Fig. 10.

The presence of noise in measurements does affect the performance of methods for identification of stiffness parameters as shown in Tables 2 and 3. The stiffness estimates for scenarios with known excitations are very accurate. For scenarios with unknown excitations, the accuracy of results deteriorates but they are still reasonable.
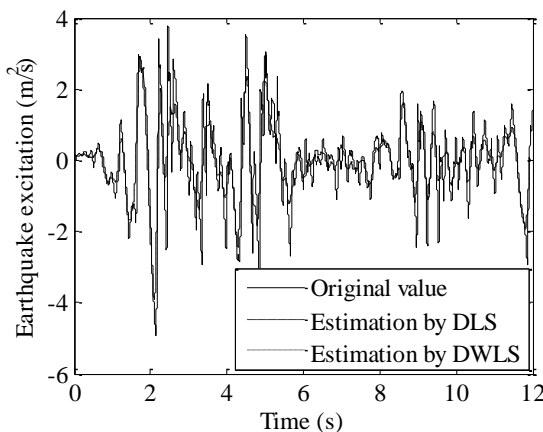

Fig. 10 Example 1: Estimated earthquake excitations (2.5% noise)

Fig. 10 shows that the estimated excitation for the scenario with unknown excitation is also acceptable. The DLS method generally performs slightly better in the perfect situation of zero noise, but for scenarios with noise when the excitation is unknown, the DWLS method works slightly better.

4.2 Example 2: A single-bay two-storey frame

A more realistic single-bay two-storey frame made up of steel W-type I-beam, as shown in Fig. 11, is then studied to verify the capability of the proposed method. The member used and their properties are shown in Table 4. The lumped mass at each beam-column joint is 50,000 kg, while the joint loads to account for gravity are $P_1 = 1000\,\text{kN}$ and $P_2 = 500\,\text{kN}$. Fig. 11 also shows an arbitrary arrangement of sensors for measurements. Each frame member is discretized into three elements by having the sensor locations as interior nodes. All other conditions and parameters are the same as those in Example 1 unless otherwise stated. The identified plastic rotations at selected plastic hinges for the zero-noise scenario as shown in Fig. 12 indicates that, in spite of the more complicated behaviour of the frame, the proposed method can identify the plastic rotations satisfactorily. The weight matrix $\mathbf{W}$ for the frame in Fig. 11 is similarly given by Eq. (24) with the sub-matrix $\overline{\mathbf{W}}_t$ to apply weights on the equations of motion of both floors given by
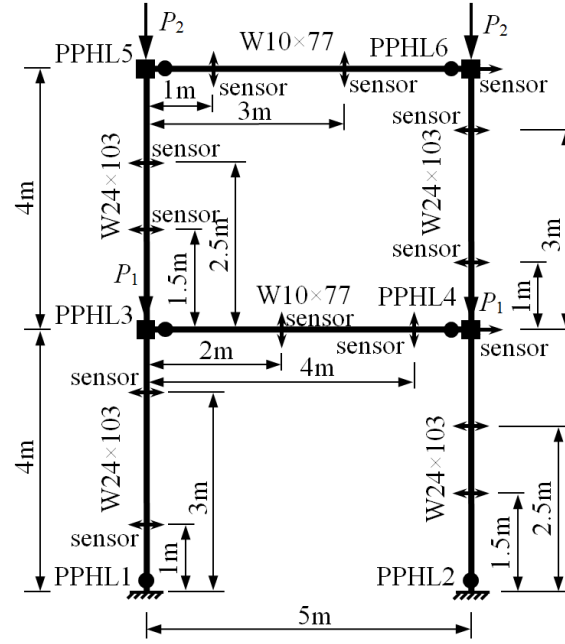
Fig. 11 Example 2: A single-bay two-storey frame (↔: sensor with measurement direction indicated)

Table 4 Example 2: Properties of steel W-type I-beams used

Member	Area (m²)	Moment of Inertia (m⁴)	Yield Moment (Nm)
Column (W24×103)	1.9548×10^{-2}	1.2487×10^{-3}	1.1379×10^{6}
Beam (W10×77)	1.4581×10^{-2}	1.8939×10^{-4}	3.9665×10^{5}

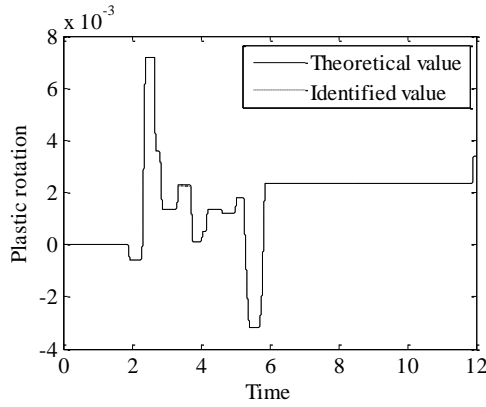Table 5 Example 2: Identified stiffness parameters (Unit: Nm; zero noise)

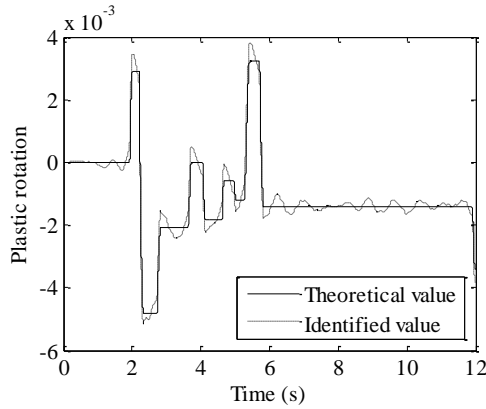|	Theoretical value	DLS with known excitation	DWLS with known excitation	DLS with unknown excitation	DWLS with unknown excitation
k_{cL1}	6.2435×10^{7}	6.2599×10^{7} (0.26%)	6.2533×10^{7} (0.16%)	6.1971×10^{7} (0.74%)	6.0891×10^{7} (2.47%)
k_{cR1}	6.2435×10^{7}	6.2335×10^{7} (0.16%)	6.2354×10^{7} (0.13%)	6.1664×10^{7} (1.23%)	6.0440×10^{7} (3.20%)
k_{b1}	0.7576×10^{7}	0.7904×10^{7} (4.33%)	0.7918×10^{7} (4.51%)	0.8227×10^{7} (8.59%)	0.8526×10^{7} (12.54%)
k_{cL2}	6.2435×10^{7}	6.2453×10^{7} (0.03%)	6.2554×10^{7} (0.19%)	6.4867×10^{7} (3.90%)	6.7120×10^{7} (7.50%)
k_{cR2}	6.2435×10^{7}	6.2232×10^{7} (0.33%)	6.2358×10^{7} (0.12%)	6.4623×10^{7} (3.50%)	6.6791×10^{7} (6.98%)
k_{b2}	0.7576×10^{7}	0.8034×10^{7} (6.05%)	0.8050×10^{7} (6.26%)	0.8344×10^{7} (10.14%)	0.8630×10^{7} (13.91%)

Note: Percentage errors are shown in parentheses

$$\bar{\mathbf{W}}_t = \begin{bmatrix} 0.1 & 0 & 0 & 0 & 0 & 0 \\ 0 & 0.1 & 0 & 0 & 0 & 0 \\ 0 & 0 & 1 & 0 & 0 & 0 \\ 0 & 0 & 0 & 0.1 & 0 & 0 \\ 0 & 0 & 0 & 0 & 0.1 & 0 \\ 0 & 0 & 0 & 0 & 0 & 1 \end{bmatrix} \quad \text{for } t = 1, 2, \cdots n_t \qquad (27)$$

The identified stiffness parameters for the zero-noise scenario are shown in Table 5 while, for the case of unknown excitation, the estimated excitations are shown in Fig. 13. As each component equation of Eq. (17) related to $D_q^d \left(q = 1, 2, \cdots, n_s \right)$ gives an estimate of the excitation, the final result can be obtained by averaging the estimates.

The accuracy of the estimated stiffness parameters for the case with known excitation is satisfactory. The relatively larger errors of the beam stiffness parameters are largely due to the assumption of zero vertical displacements at beam-column joints, which also causes fluctuations in the identified plastic rotations at plastic hinges formed in beams. Understandably the accuracy drops for the case with unknown excitation, but the results are still acceptable. Fig. 13 shows that the estimated excitation for the zero-noise scenario is very accurate.
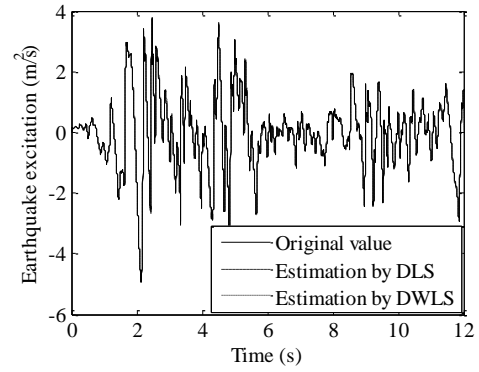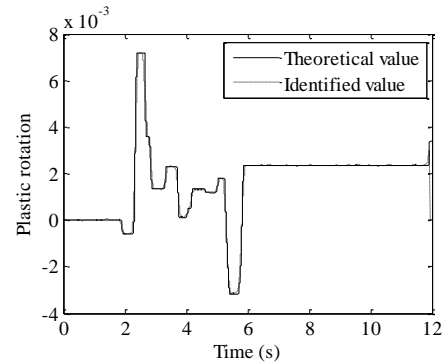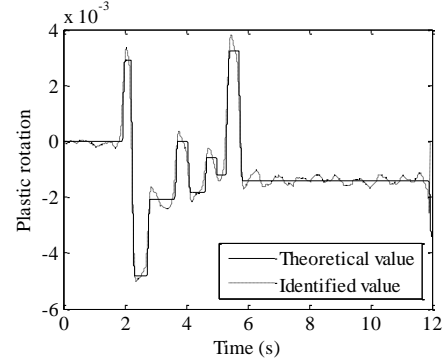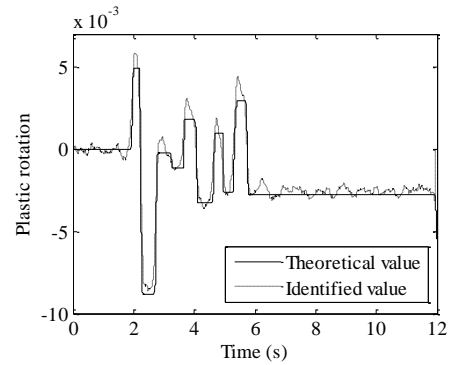
Fig. 13 Example 2: Estimated earthquake excitations (zero-noise scenario)
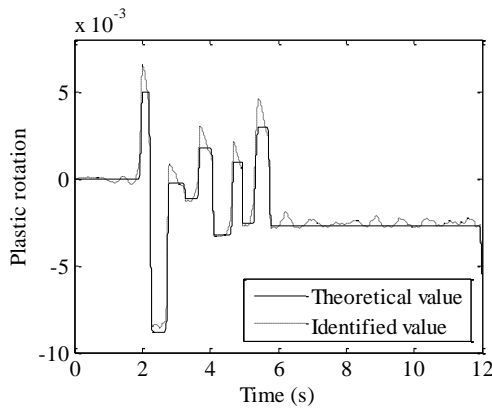
(a) PPHL1

(b) PPHL3

(c) PPHL5

Fig. 12 Example 2: Plastic rotations at selected plastic hinges (zero–noise scenario)

Fig. 14 Example 2: Plastic rotations at selected plastic hinges (2.5% noise)

Table 6 Example 2: Identified stiffness parameters (Unit: Nm; 2.5% noise)

	Theoretical value	DLS with known excitation	DWLS with known excitation	DLS with unknown excitation	DWLS with unknown excitation
k_{cL1}	6.2435×10^7	5.8994×10^7 (5.51%)	5.9578×10^7 (4.58%)	5.6574×10^7 (9.39%)	6.2453×10^7 (0.03%)
k_{cR1}	6.2435×10^7	6.2901×10^7 (0.75%)	6.4630×10^7 (3.52%)	5.9381×10^7 (4.89%)	5.4959×10^7 (11.97%)
k_{b1}	0.7576×10^7	0.6325×10^7 (16.51%)	0.7488×10^7 (1.16%)	0.6605×10^7 (12.82%)	0.7930×10^7 (4.67%)
k_{cL2}	6.2435×10^7	4.8361×10^7 (22.54%)	5.5961×10^7 (10.37%)	5.0171×10^7 (19.64%)	5.8224×10^7 (6.74%)
k_{cR2}	6.2435×10^7	5.1757×10^7 (17.10%)	6.1590×10^7 (1.35%)	5.3807×10^7 (13.82%)	6.5514×10^7 (4.93%)
k_{b2}	0.7576×10^7	0.6445×10^7 (14.93%)	0.7565×10^7 (0.15%)	0.6694×10^7 (11.64%)	0.7962×10^7 (5.10%)

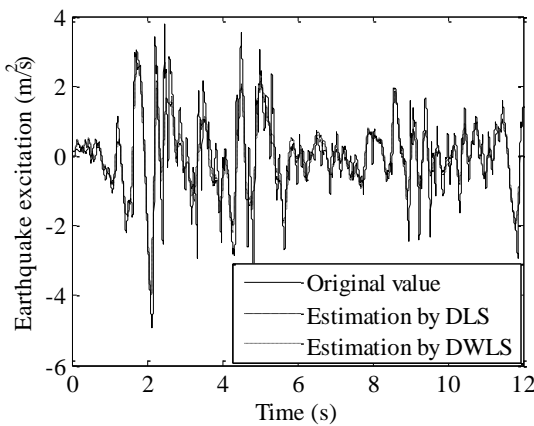Note: Percentage errors are shown in parentheses

Fig. 15 Example 2: Estimated earthquake excitations (2.5% noise)

To investigate the feasibility of the proposed method, 2.5% noise is added to the simulated measurements while all other conditions are the same as before. The identified plastic rotations at selected plastic hinges are shown in Fig. 14, confirming that the proposed method works with measurements contaminated with noise. Table 6 shows that the estimated stiffness parameters from the DWLS method are much better than those from the DLS method for both the cases with known and unknown excitations. As before, the DWLS method is good at dealing with the scenarios with measurement noise. The measurement noise tends to propagate and adversely affects the elastic rotations estimated. Through the noise-removal technique and the DWLS method, the stiffness parameters can be estimated with satisfactory accuracy for both the cases with known and unknown excitations. Fig. 15 shows that, for the case of unknown excitation, the proposed method can estimate the excitation with reasonable accuracy.

5. Conclusions

This paper has proposed a novel method to identify the properties of nonlinear single-bay frames with hysteretic plastic hinges. In particular, the structure is decomposed into linear and nonlinear parts, so that the nonlinear effects can be considered separately for estimation of the parameters of linear members. The proposed method can give the plastic rotations which furnish information of the locations and plasticity degrees of plastic hinges. For stiffness parameter estimation in the zero-noise situation with known excitation, the results for the beams are less accurate than those for the columns. In scenarios with higher measurement noise, the accuracy tends to suffer but adoption of suitable correction method helps. In comparison, the damped-and-weighted-least-squares method performs better than damped-least-squares method for estimation of stiffness parameters from noise-contaminated responses. Even with scenarios having unknown excitations, both the stiffness parameters and ground excitation can be estimated with acceptable accuracy.

References

Al-Hussein, A. and Haldar, A. (2015a), "Novel unscented Kalman filter for health assessment of structural systems with unknown input", *J. Eng. Mech. - ASCE*, **141**(7), 04015012.

Al-Hussein, A. and Haldar, A. (2015b), "Structural health assessment at a local level using minimum information", *Eng. Struct.*, **88**, 100-110.

Au, F.T.K., Jiang, R.J. and Cheung, Y.K. (2004), "Parameter identification of vehicles moving on continuous bridges", *J. Sound Vib.*, **269**(1-2), 91-111.

Au, F.T.K. and Yan, Z.H. (2008), "Dynamic analysis of frames with material and geometric nonlinearities based on the semirigid technique", *Int. J. Struct. Stab. Dynam.*, **8**(3), 415-438.

Burak, S. and Ram, Y.M. (2001), "Construction of physical parameters from modal data", *Mech. Syst. Signal Pr.*, **15**(1), 3-10.

Chakraverty, S. (2005), "Identification of structural parameters of multistorey shear buildings from modal data", *Earthq. Eng. Struct. D.*, **34**(6), 543-554.

Gindy, M., Nassif, H.H. and Velde, J. (2016), "Bridge displacement estimates from measured acceleration records", *Transportation Research Record: Journal of the Transportation Research Board, No. 2028*, Transportation Research Board of the National Academies, Washington, D.C., 2007, 136-145.

Hasan, R., Xu, L. and Grierson, D.E. (2002), "Push-over analysis for performance-based seismic design", *Comput. Struct.*, **80**(31), 2483-2493.

Huang, H., Yang, Y. and Sun, L. (2015), "Parametric identification of a cable-stayed bridge using least square estimation with substructure approach", *Smart Struct. Syst.*, **15**(2), 425-445.

Kang, J.S., Park, S.K., Shin, S. and Lee, H.S. (2005), "Structural system identification in time domain using measured acceleration", *J. Sound Vib.*, **288**(1-2), 215-234.

Lu, Z.R. and Law, S.S. (2007), "Identification of system parameters and input force from output only", *Mech. Syst. Signal Pr.*, **21**(5), 2099-2111.

Monforton, G.R. and Wu, T.S. (1963), "Matrix analysis of semi-rigidly connected frames", *J. Struct. Div.- ASCE*, **89**(6), 13-42.

Nagarajaiah, S. and Yang, Y. (2015), "Blind modal identification of output-only non-proportionally-damped structures by time-frequency complex independent component analysis", *Smart Struct. Syst.*, **15**(1), 81-97.

Park, J.H., Kim, J.T. and Yi, J.H. (2011), "Output-only modal identification approach for time-unsynchronized signals from decentralized wireless sensor network for linear structural systems", *Smart Struct. Syst.*, **7**(1), 59-82.

Park, S.K., Park, H.W., Shin, S. and Lee, H.S. (2008), "Detection of abrupt structural damage induced by an earthquake using a moving time window technique", *Comput. Struct.*, **86**(11-12), 1253-1265.

Shi, Z.Y., Law, S.S. and Li, H.N. (2007), "Subspace-based identification of linear time-varying system", *AIAA Journal*, **45**(8), 2042-2050.

Tikhonov, A.N. (1963), "Solution of incorrectly formulated problems and the regularization method", *Soviet Mathematics*, **4**, 1035-1038.

Wang, C., Ren, W.X., Wang, Z.C. and Zhu, H.P. (2014), "Time-varying physical parameter identification of shear type structures based on discrete wavelet transform", *Smart Struct. Syst/*, **14**(5), 831-845.

Yang, J., Huang, H.W. and Pan, S.W. (2009), "Adaptive quadratic sum-squares error for structural damage identification", *J. Eng. Mech. - ASCE*, **135**(2), 67-77.

Yang, J., Xia, Y. and Loh, C. (2014a), "Damage detection of hysteretic structures with a pinching effect', *J. Eng. Mech.-ASCE*, **140**(3), 462-472.

Yang, J.N., Xia, Y. and Loh, C.H. (2014b), "Damage identification of bolt connections in a steel frame", *J. Struct. Eng. - ASCE*, **140**(3), 04013064.

Yang, Y.B., Li, Y.C. and Chang, K.C. (2014), "Constructing the mode shapes of a bridge from a passing vehicle: a theoretical study", *Smart Struct. Syst.*, **13**(5), 797-819.

Ye, X., Yan, Q., Wang, W. and Yu, X. (2012), "Modal identification of Canton Tower under uncertain environmental conditions", *Smart Struct. Syst.*, **10**(4), 353-373.

Zhang, J., Yan, R.Q. and Yang, C.Q. (2013), "Structural modal identification through ensemble empirical modal decomposition", *Smart Struct. Syst.*, **11**(1), 123-134.

HJ